Numerical simulation of a non-charring ablator in high-enthalpy flows by means of a unified flow-material solver

P. Schrooyen[1], **J. Coheur**[2,3], A. Turchi[3], K. Hillewaert[1], P. Chatelain[4], T. Magin[3]

[1]Cenaero, Gosselies, Belgium
[2]Université de Liège, Liège, Belgium
[3]von Karman Institute for Fluid Dynamics, Brussels, Belgium
[4]Université Catholique de Louvain-la-Neuve, Louvain-la-Neuve, Belgium

47th AIAA Thermophysics Conference, June 5–9, 2017
Denver, Colorado, USA
TP-02, Ablation I

Atmospheric reentry: a complex multiphysics problem

- Need for accurate characterization of TPS for maximizing payload, ensuring safety and the success of the mission

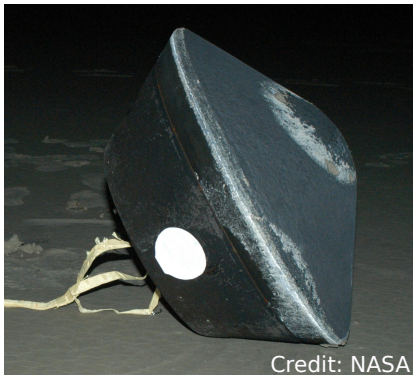
Credit: NASA

Atmospheric reentry: a complex multiphysics problem

- Need for accurate characterization of TPS for maximizing payload, ensuring safety and the success of the mission

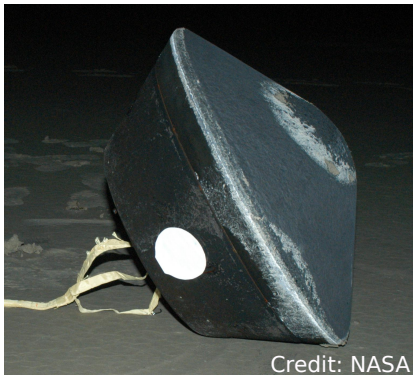

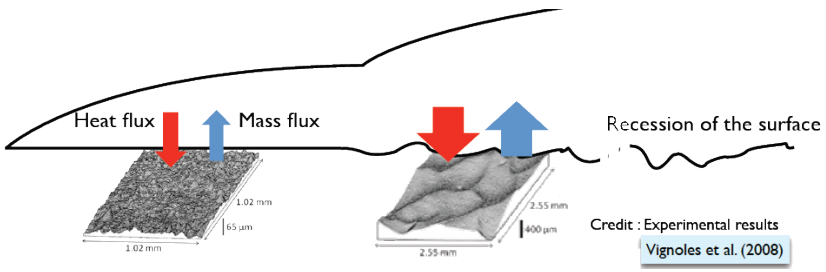

- Typical mission killers
  - ➔ Non-equilibrium effects in the shock and boundary layers
  - ➔ Gas-surface interactions
  - ➔ Flow-transition from laminar to turbulent

- Our goal: develop higher fidelity tools to model those mission killers and better assist TPS design

Atmospheric reentry: a complex multiphysics problem

- Need for accurate characterization of TPS for maximizing payload, ensuring safety and the success of the mission

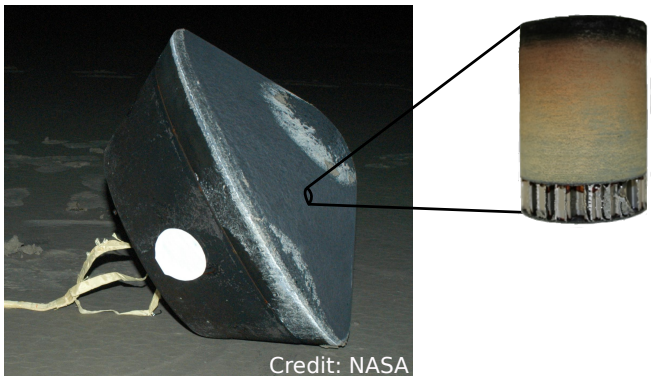

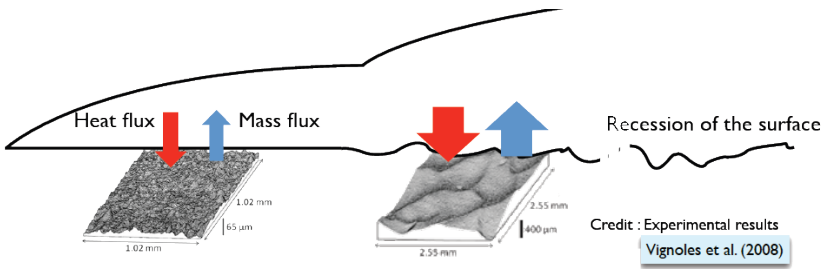

- Typical mission killers
  - ➔ Non-equilibrium effects in the shock and boundary layers
  - ➔ Gas-surface interactions
  - ➔ Flow-transition from laminar to turbulent

- Our goal: develop higher fidelity tools to model those mission killers and better assist TPS design

Gas-surface interactions: in-depth ablation

- Numerical simulations (Schrooyen et al., 2016) of the NASA side-arm experiments (Panerai et al., 2014) showed the importance of volume ablation in porous materials for such flow conditions

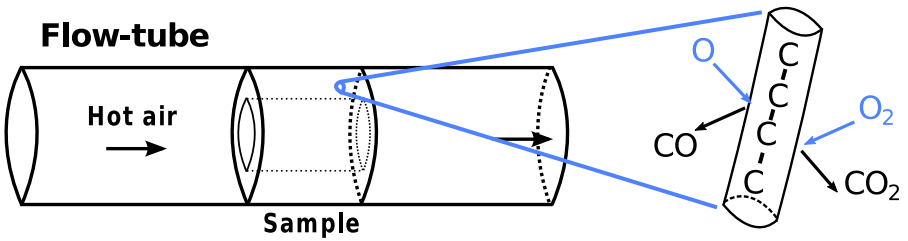

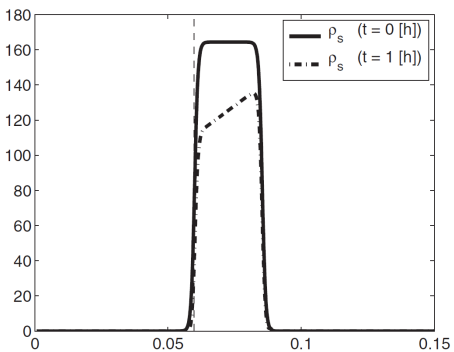

Volume ablation vs. surface ablation ➔ Thiele number

$$Th = \frac{L}{\sqrt{D_{\text{eff}}/(S_f k_f)}}$$

- The simulation tool, although suitable for studying volume ablation, is shown here to reproduce also VKI Plasmatron experiments where surface ablation dominates

Table of Contents

Table of Contents

Materials for TPS design

- Ablative thermal protection materials (TPMs) will allow future sample return missions and high speed re-entries!
- Investigated here: lightweight, **highly porous** ablative materials (like PICA in the US, Asterm in the EU)

Carbon preform

Credit: Mersen Scotland

Carbon/phenol composite

Credit: Airbus DS

- Carbon/phenol material = **Carbon preform** + phenolic resin

Pyrolysis-ablation problem

- When heated, the TPM is transformed and removed by two phenomena
  - pyrolysis ➔ thermal decomposition
  - ablation ➔ gas-solid reactions and transport of products, sublimation, spallation

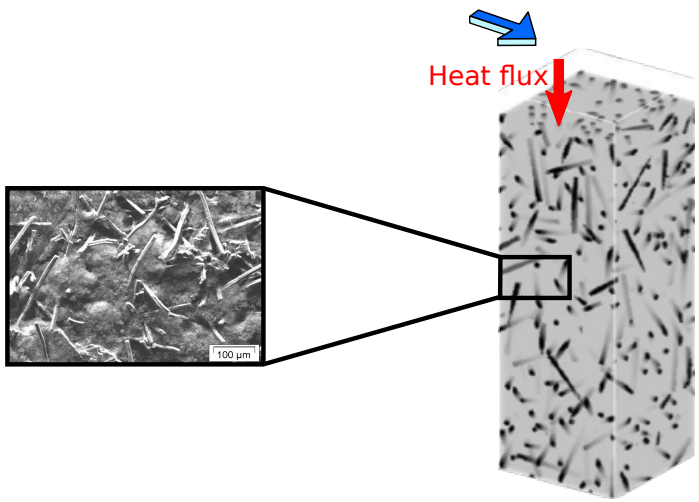

Credits: (left) Stackpoole *et al.* (2010)
(right) Lachaud *et al.* (2008)

Pyrolysis-ablation problem

- When heated, the TPM is transformed and removed by two phenomena
  - pyrolysis ➔ thermal decomposition
  - ablation ➔ gas-solid reactions and transport of products, sublimation, spallation

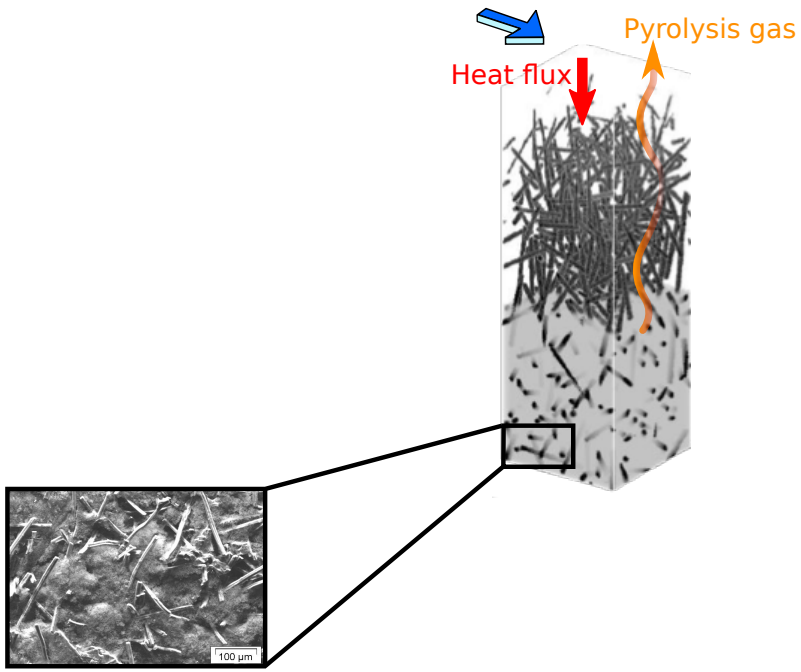

Credits: (left) Stackpoole *et al.* (2010)
(right) Lachaud *et al.* (2008)

4. Partially ablated
3. Charred
2. Partially pyrolyzed
1. Virgin material

Pyrolysis-ablation problem

- When heated, the TPM is transformed and removed by two phenomena
  - pyrolysis ➔ thermal decomposition
  - ablation ➔ gas-solid reactions and transport of products, sublimation, spallation

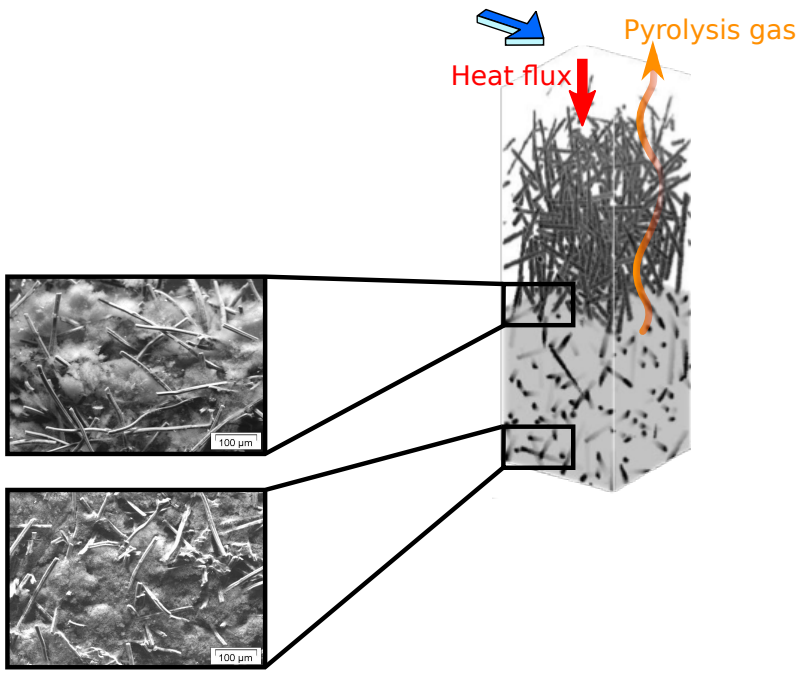

Credits: (left) Stackpoole *et al.* (2010)
(right) Lachaud *et al.* (2008)

4. Partially ablated
3. Charred
2. Partially pyrolyzed
1. Virgin material

Pyrolysis-ablation problem

- When heated, the TPM is transformed and removed by two phenomena
  - pyrolysis ➔ thermal decomposition
  - ablation ➔ gas-solid reactions and transport of products, sublimation, spallation

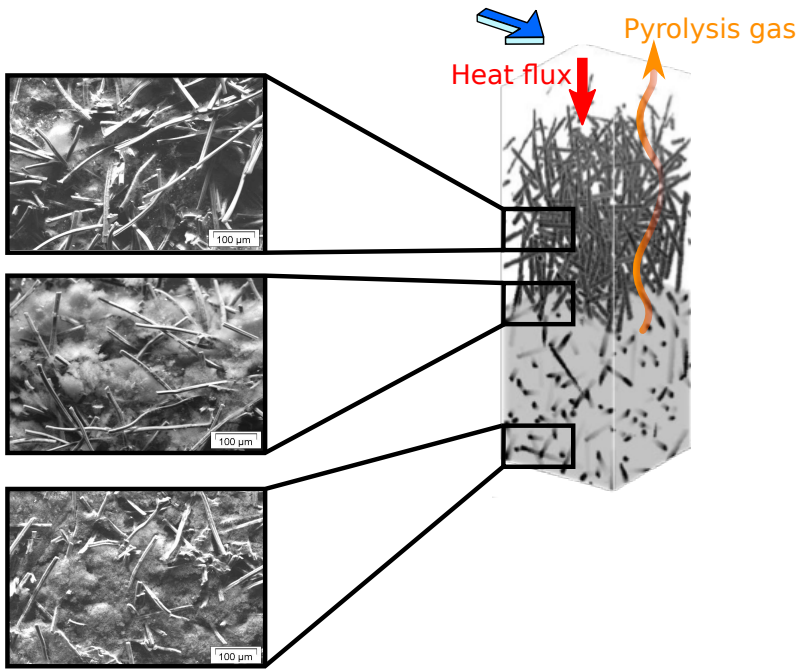

Credits: (left) Stackpoole *et al.* (2010)
(right) Lachaud *et al.* (2008)

4. Partially ablated
3. Charred
2. Partially pyrolyzed
1. Virgin material

Pyrolysis-ablation problem

- When heated, the TPM is transformed and removed by two phenomena
  - pyrolysis ➔ thermal decomposition
  - ablation ➔ gas-solid reactions and transport of products, sublimation, spallation

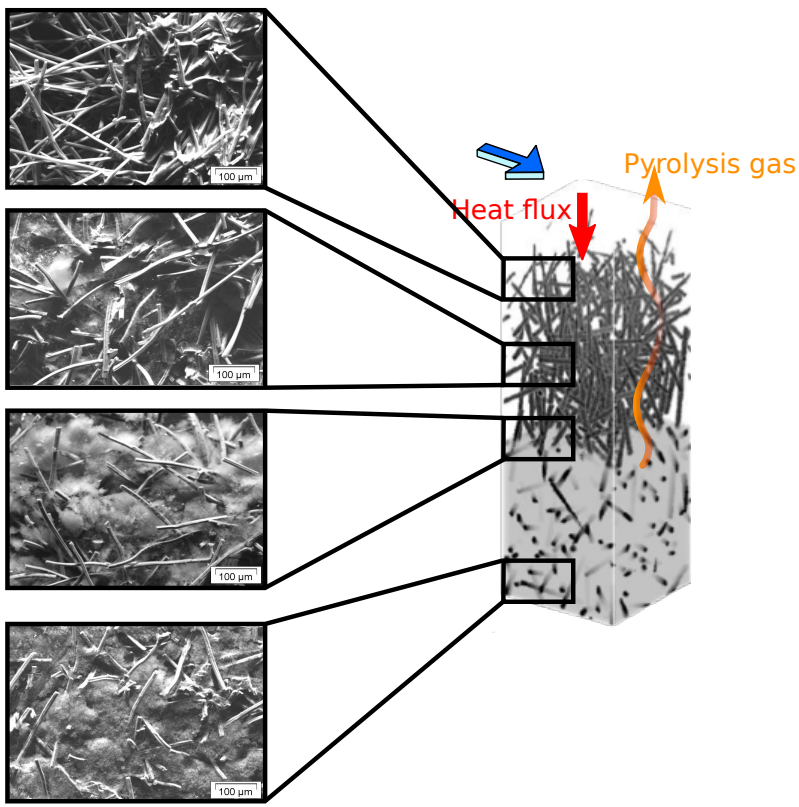

Credits: (left) Stackpoole *et al.* (2010)
(right) Lachaud *et al.* (2008)

4. Partially ablated
3. Charred
2. Partially pyrolyzed
1. Virgin material

Pyrolysis-ablation problem

- When heated, the TPM is transformed and removed by two phenomena
  - pyrolysis ➔ thermal decomposition: tomorrow (TP-04, Ablation II)
  - ablation ➔ gas-solid reactions and transport of products: today

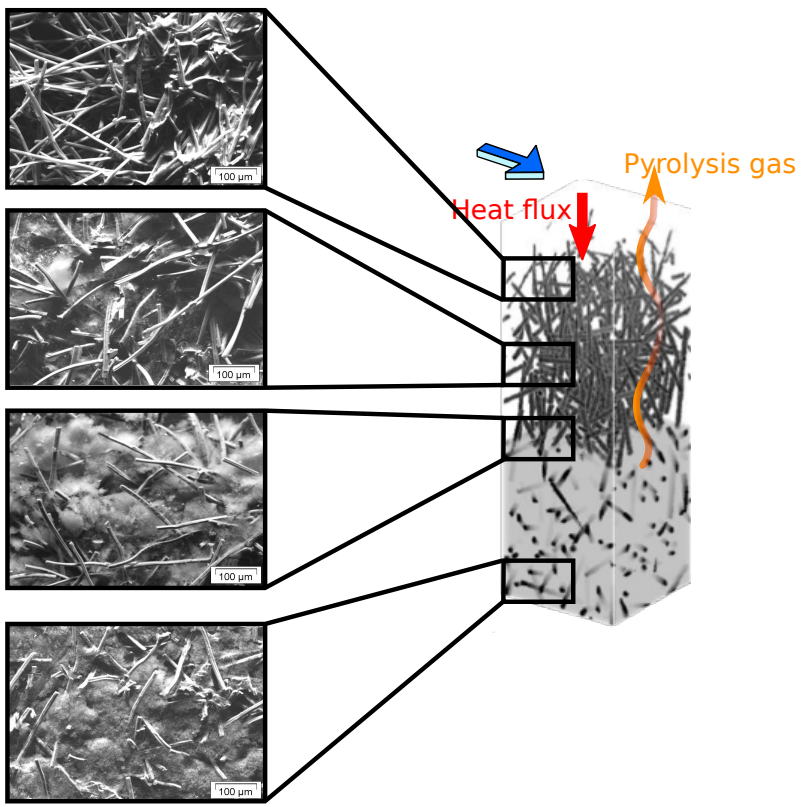

Credits: (left) Stackpoole *et al.* (2010)
(right) Lachaud *et al.* (2008)

4. Partially ablated
3. Charred
2. Partially pyrolyzed
1. Virgin material

Strategies for studying gas-surface interaction

Ground test facilities

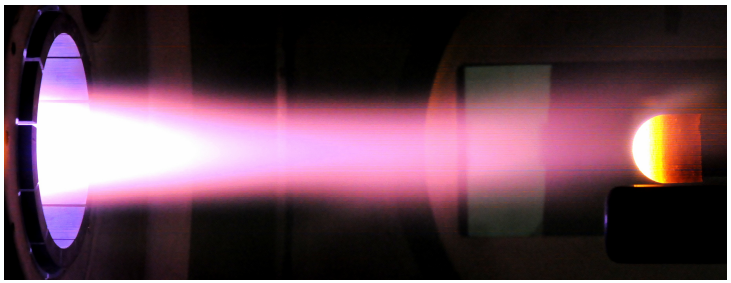

VKI Plasmatron test on carbon-phenolic
B. Helber, 2016

Numerical simulations

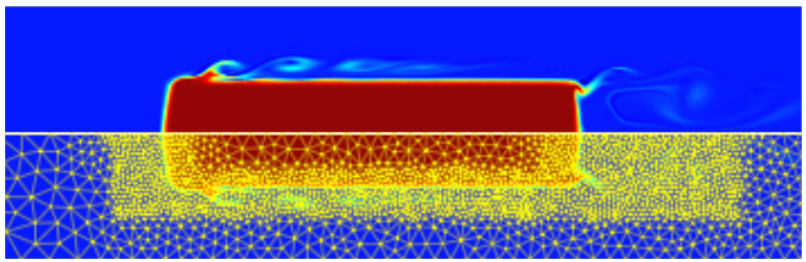

Unified flow-material approach
P. Schrooyen, 2015

Strategies for studying gas-surface interaction

Ground test facilities

VKI Plasmatron test on carbon-phenolic
B. Helber, 2016

Numerical simulations

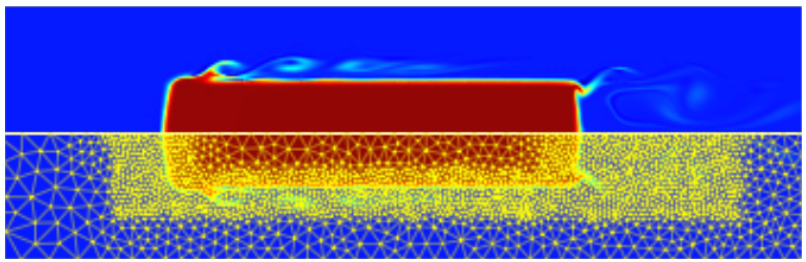

Unified flow-material approach
P. Schrooyen, 2015

Numerical approaches for studying ablation

① CFD code with ablative boundary conditions

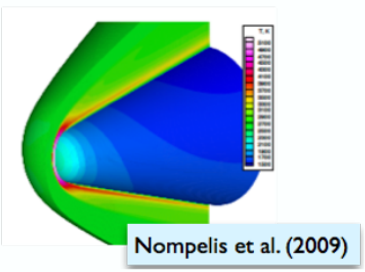

Nompelis et al. (2009)

② Material response code with heat transfer coefficients

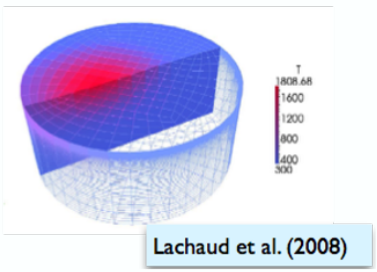

Lachaud et al. (2008)

③ Loosely coupled approach

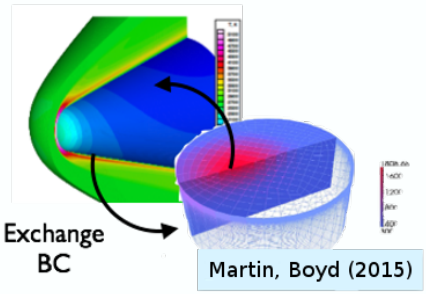

Martin, Boyd (2015)

④ **Unified approach**

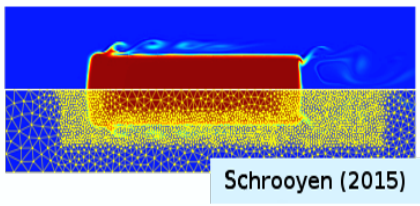

Schrooyen (2015)

Strategies for studying gas-surface interaction

Ground test facilities

VKI Plasmatron test on carbon-phenolic
B. Helber, 2016

Numerical simulations

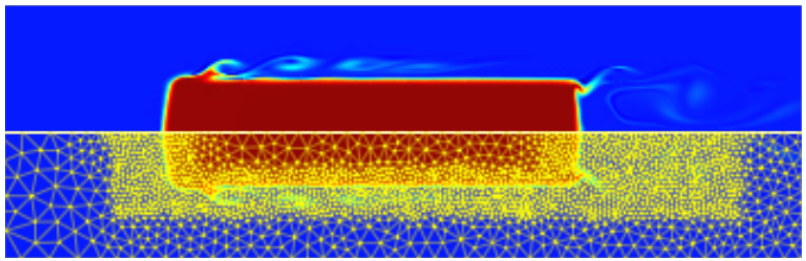

Unified flow-material approach
P. Schrooyen, 2015

Numerical approaches for studying ablation

1. CFD code with ablative boundary conditions

Nompelis et al. (2009)

2. Material response code with heat transfer coefficients

Lachaud et al. (2008)

3. Loosely coupled approach

Martin, Boyd (2015)

4. **Unified approach**

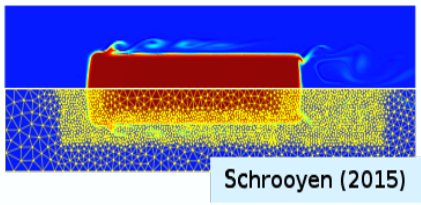

Schrooyen (2015)

Table of Contents

How to treat multiphase flows?

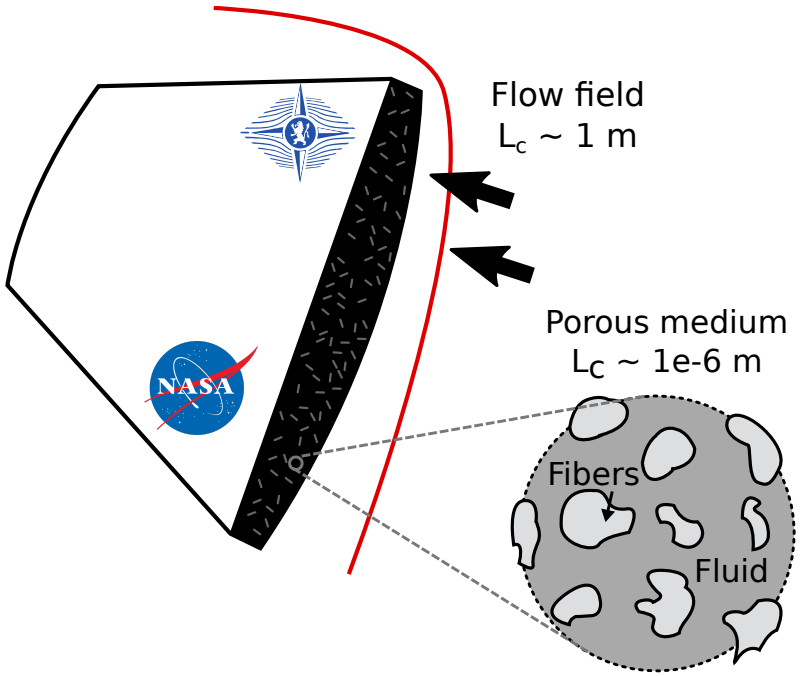

- Navier-Stokes equations for multicomponent flows valid everywhere in the fluid phase
- Chemical reactions with the solid phase

➔ Resolution too costly!

➔ Coupling the solid phase(s) with CFD not easy!

- Perform local volume averaging for a "more homogeneous" description (mesoscopic scale)
- New set of PDEs valid everywhere in the domain: Volume-Averaged Navier-Stokes (VANS) equations and chemical reaction laws

VANS equations for non-pyrolyzing media

Mass

$$\partial_t \left(\varepsilon_{\mathrm{g}} \langle \rho_i \rangle_{\mathrm{g}}\right) + \mathrm{div}_{\mathbf{x}} \left(\varepsilon_{\mathrm{g}} \langle \rho_i \rangle_{\mathrm{g}} \langle \boldsymbol{u} \rangle_{\mathrm{g}}\right) =$$
$$-\mathrm{div}_{\mathbf{x}} \langle \boldsymbol{J}_i \rangle + \langle \dot{\omega_i}^{\mathrm{hom}} \rangle + \langle \dot{\omega_i}^{\mathrm{het}} \rangle \quad (1)$$
$$\partial_t \langle \rho_{\mathrm{s}} \rangle = -\langle \dot{\omega}^{\mathrm{het}} \rangle \quad (2)$$

Momentum

$$\partial_t (\varepsilon_{\mathrm{g}} \langle \rho \boldsymbol{u} \rangle_{\mathrm{g}}) + \mathrm{div}_{\mathbf{x}} (\varepsilon_{\mathrm{g}} \langle \rho \rangle_{\mathrm{g}} \langle \boldsymbol{u} \rangle_{\mathrm{g}} \langle \boldsymbol{u} \rangle_{\mathrm{g}}) =$$
$$-\varepsilon_{\mathrm{g}} \nabla \langle p \rangle_{\mathrm{g}} + \mathrm{div}_{\mathbf{x}} \langle \boldsymbol{\tau} \rangle + \boldsymbol{F}_{\mathbf{gs}} \quad (3)$$

Energy

$$\partial_t \langle \rho E_{\mathrm{tot}} \rangle + \mathrm{div}_{\mathbf{x}} (\varepsilon_{\mathrm{g}} \langle \rho \rangle_{\mathrm{g}} \langle H \rangle_{\mathrm{g}} \langle \boldsymbol{u} \rangle_{\mathrm{g}})$$
$$= \mathrm{div}_{\mathbf{x}} (k_{\mathrm{eff}} \nabla \langle T \rangle) + \mathrm{div}_{\mathbf{x}} (\langle \boldsymbol{\tau} \cdot \boldsymbol{u} \rangle) \quad (4)$$

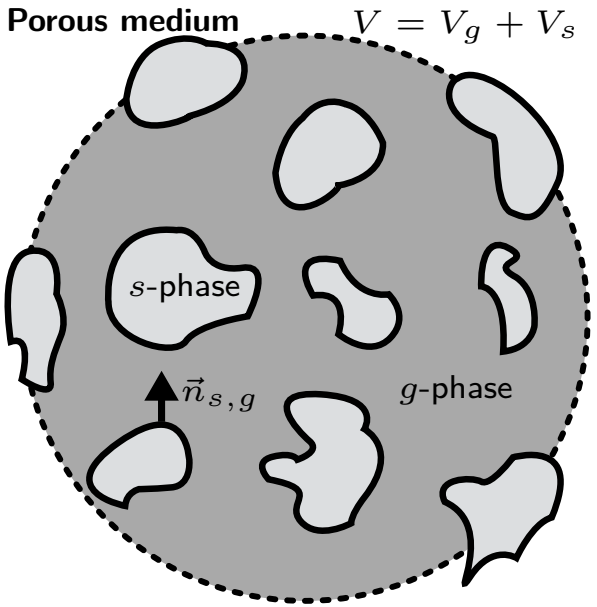

- Volume fractions

$$\varepsilon_{\mathrm{g}} = \frac{V_{\mathrm{g}}}{V}, \quad \varepsilon_{\mathrm{s}} = 1 - \varepsilon_{\mathrm{g}}$$

- Intrinsic average operator

$$\langle \alpha \rangle_\gamma = \frac{1}{V_\gamma} \int_{V_\gamma} \alpha \, dV$$

Heterogeneous chemical reactions

$$\langle \dot{\omega}_i^{\text{het}} \rangle = \frac{1}{dV} \oint_{\partial\Omega_g} \underbrace{k_f^{i,C(s)} \langle \rho_i \rangle_{\text{gs}}}_{\text{constant along fiber surface}} \, dS$$

$$= k_f^{i,C(s)} \langle \rho_i \rangle_{\text{gs}} \underbrace{\frac{1}{dV} \oint_{\partial\Omega_g} dS}_{=A_{\text{w}}/dV \equiv S_f}$$

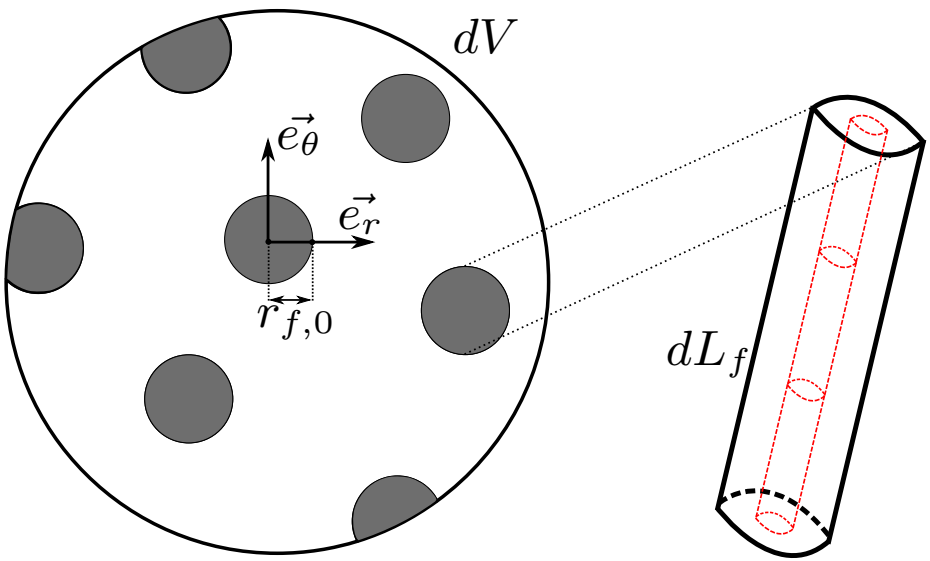

Cylindrical recession

$$S_f = \frac{2}{r_{f,0}} \sqrt{\varepsilon_{s,0} \varepsilon_s}$$

Non-constant fiber reactivity

$$S_f = \gamma \frac{A_w}{dV}$$

(see Schrooyen et al., 2016)

Table of Contents

Numerical modeling

- DGAblation module of Argo
- Space discretization: Discontinuous Galerkin Method (DGM)

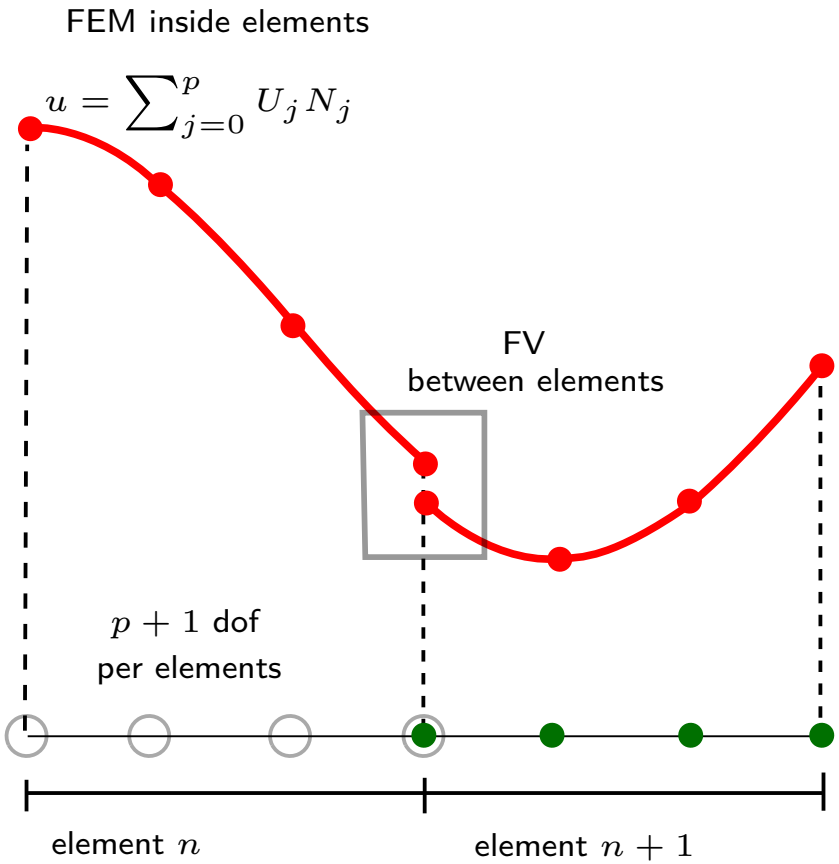

- Local conservation of physical quantities
- High order of accuracy
- Low numerical dissipation and dispersion
- Fully implicit

Hillewaert (2013), Schrooyen (2015).

Weak formulation of the convection-diffusion-reaction problem

$$\forall v \in \mathcal{V}, \quad \forall m \in N_v, \quad \int_\Omega v \mathcal{L}_m(u) d\Omega = 0 = \underbrace{\sum_{\Omega_e \in \Omega} \int_{\Omega_e} v \frac{\partial u_m}{\partial t} d\Omega_e}_{T_v}$$

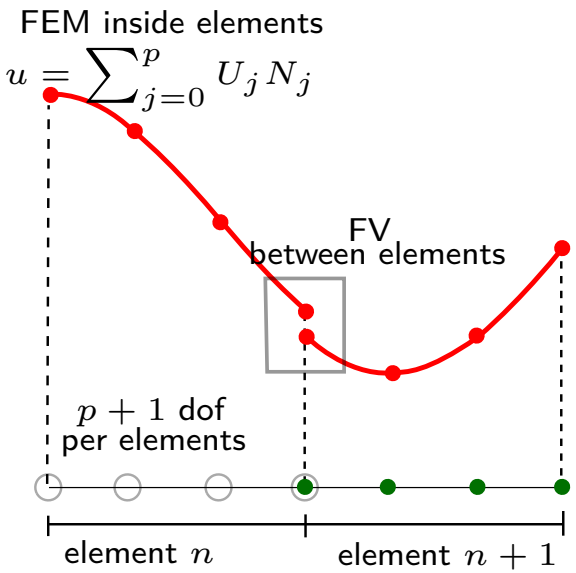

Schrooyen et al. (2016)

$$- \underbrace{\sum_{\Omega_e \in \Omega} \int_{\Omega_e} \frac{\partial v}{\partial x^k} F_m^{c,k}(\boldsymbol{u}) d\Omega_e}_{C_v} + \underbrace{\sum_{I_i \in I} \oint_{I_i} [v]^k \, n^k \mathcal{H}_m(\boldsymbol{u}^+, \boldsymbol{u}^-, \boldsymbol{n}) dS}_{C_i}$$

$$+ \underbrace{\sum_{\Omega_e \in \Omega} \int_{\Omega_e} \frac{\partial v}{x^k} (F_m^{d,k}(\boldsymbol{u})) d\Omega_e}_{D_v} - \underbrace{\sum_{I_i \in I} \oint_{I_i} \langle D_{mn}^{kl} \frac{\partial \boldsymbol{u_n}}{\partial x^l} \rangle \, [v]^k \, dS}_{D_i}$$

$$- \underbrace{\theta \sum_{I_i \in I} \oint_{I_i} \langle D_{mn}^{kl} \frac{\partial v}{\partial x^l} \rangle \, [u_m]^k \, dS}_{D_t} + \underbrace{\alpha \sum_{I_i \in I} \oint_{I_i} [v]^k \, [u_m]^k \, dS}_{D_p}$$

$$- \underbrace{\sum_{\Omega_e \in \Omega} \int_{\Omega_e} v S(\boldsymbol{u}, \nabla \boldsymbol{u}) d\Omega_e}_{S_v}$$

Table of Contents

VKI 1.2 MW Plasmatron wind tunnel

- Most powerful inductively-coupled plasma facility in the world

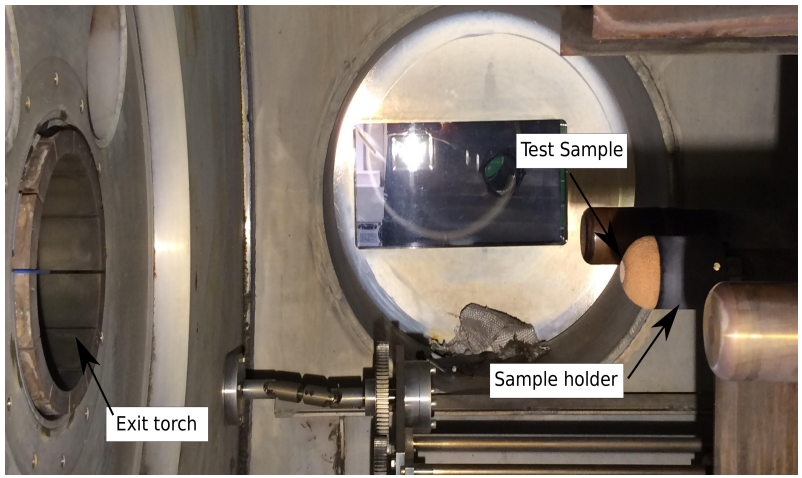

Test chamber

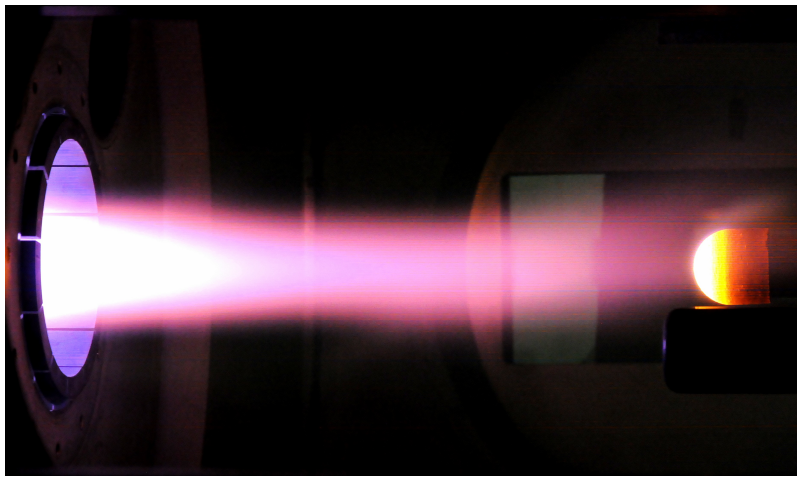

Test on a carbon-phenolic

- Test case under consideration: carbon preform sample (Helber, 2016)

Test name	gas	p_s hPa	$\dot{q}_{cw}$ kW/m^2	τ s	T_w K	$\dot{s}$ μm/s	$\dot{m}$ mg/s
HS-A2a	air	200	1050	91.2	1975	45 ± 1.4	53.2

Definition of BC and material properties

- **Plasmatron 200 hPa, 1 MW/m^2 experiment**

Material properties

- Carbon preform
- Hemispherical shape ($R = 25$ mm)
- Porosity $= 0.9$
- Permeability $= 1.45$e-10
- Tortuosity $= 1.1$
- Emissivity $= 0.86$

Credit: Mersen Scotland

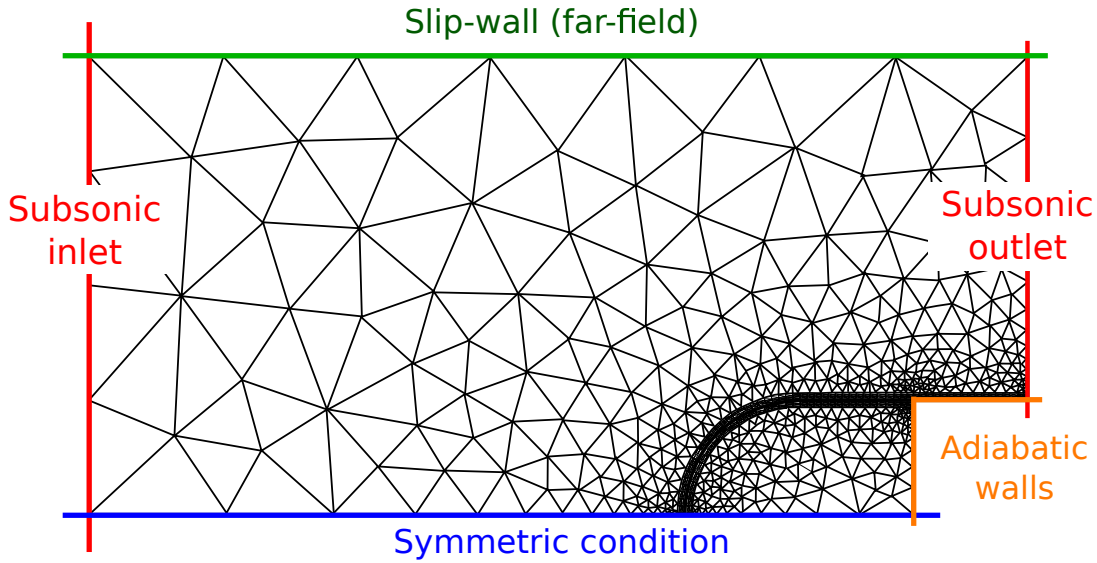

Boundary conditions

- Inlet: $U_{\text{in}} = 37$ m/s, $T_{\text{in}} = 6088$ K, Air$_5$ (O, O$_2$, N, N$_2$, NO) at T_{in}
- Outlet: $p_{\text{out}} = 200$ hPa
- Holder: adiabatic walls

Surface recession and temperature

Nb of time steps	Nb of elemts	Nb of DOFs	Nb of threads	CPU time
17100	2644	$2644 \times 10 \times 2$ $(= 158640)$	4	$\approx$ 2 days

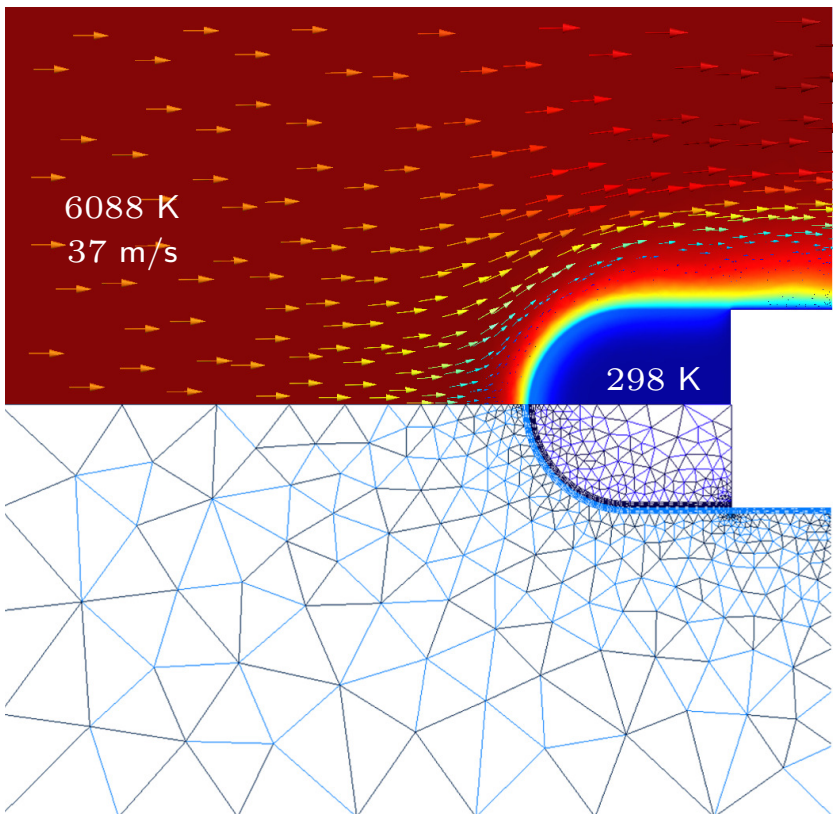

Temperature and vector flow field

Surface recession and temperature

Nb of time steps	Nb of elemts	Nb of DOFs	Nb of threads	CPU time
17100	2644	$2644 \times 10 \times 2$ $(= 158640)$	4	$\approx$ 2 days

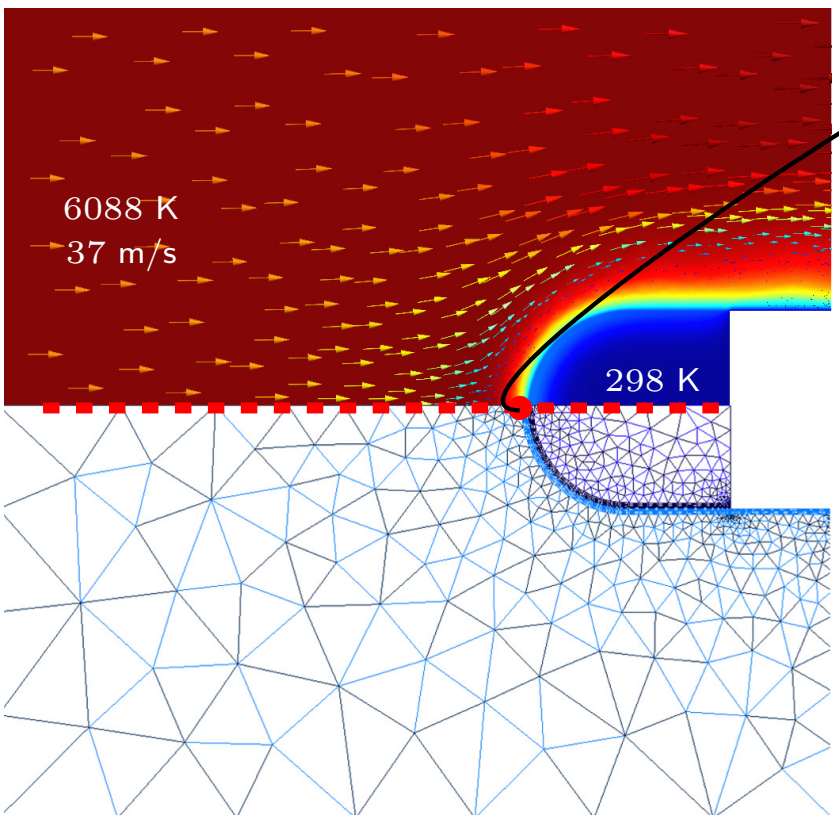

Temperature and vector flow field

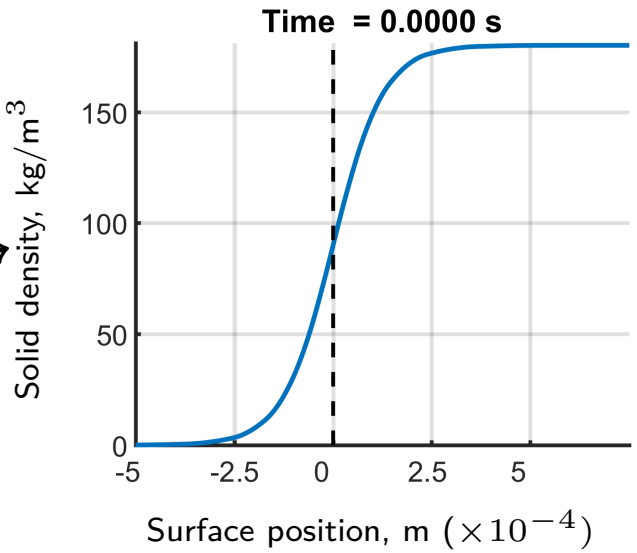

Surface recession and temperature

Nb of time steps	Nb of elemts	Nb of DOFs	Nb of threads	CPU time
17100	2644	$2644 \times 10 \times 2$ $(= 158640)$	4	$\approx$ 2 days

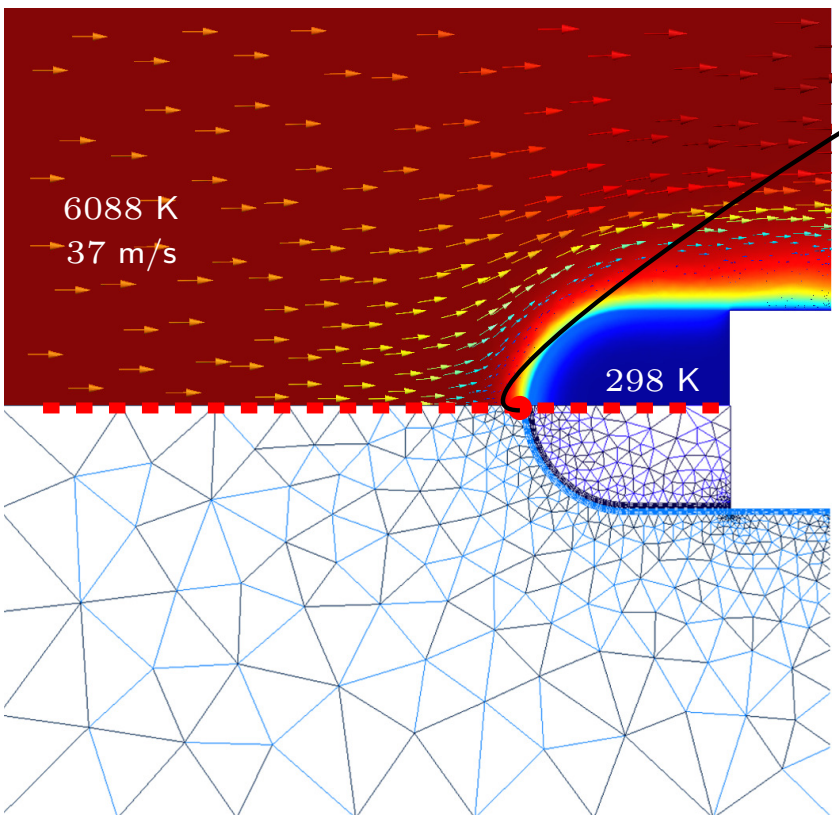

Temperature and vector flow field

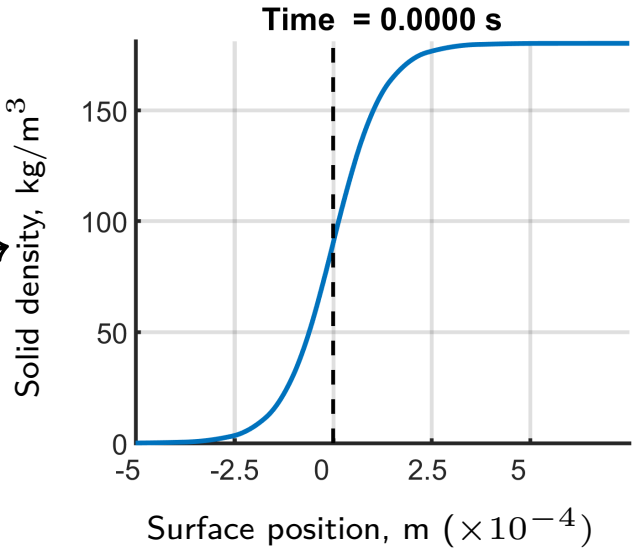

Surface recession and temperature

Nb of time steps	Nb of elemts	Nb of DOFs	Nb of threads	CPU time
17100	2644	$2644 \times 10 \times 2$ $(= 158640)$	4	$\approx$ 2 days

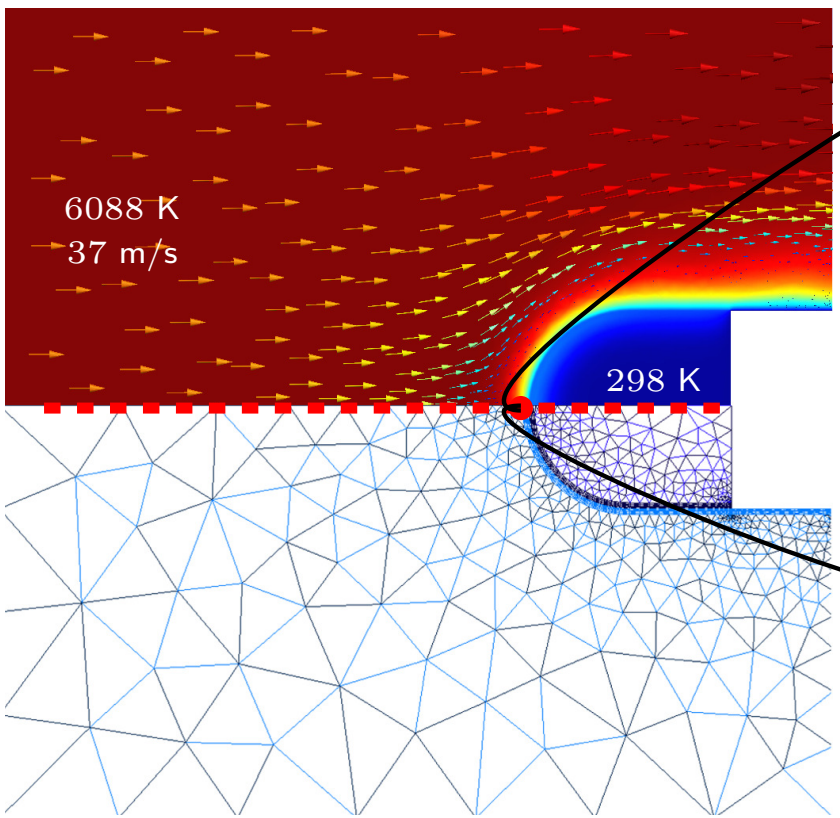

Temperature and vector flow field

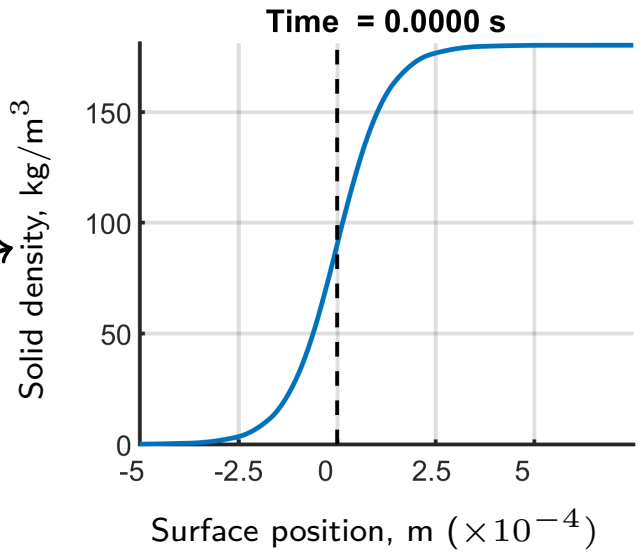

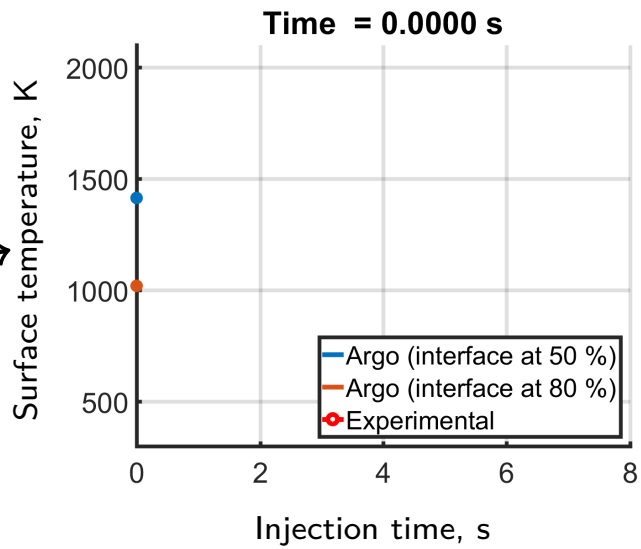

Surface recession, mass loss and material flow field

- Comparison with experimental data

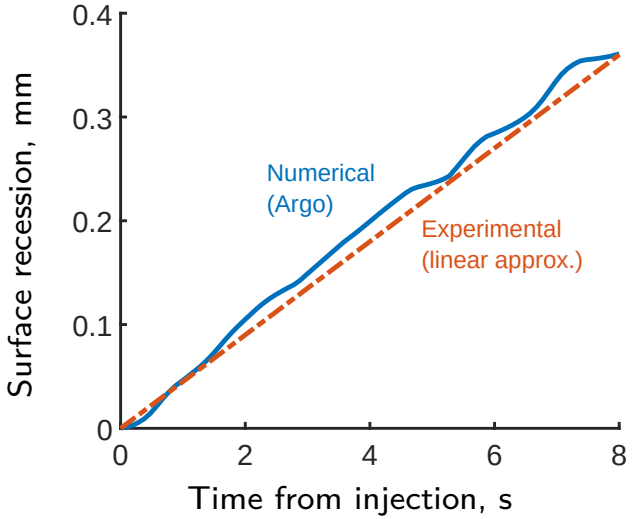

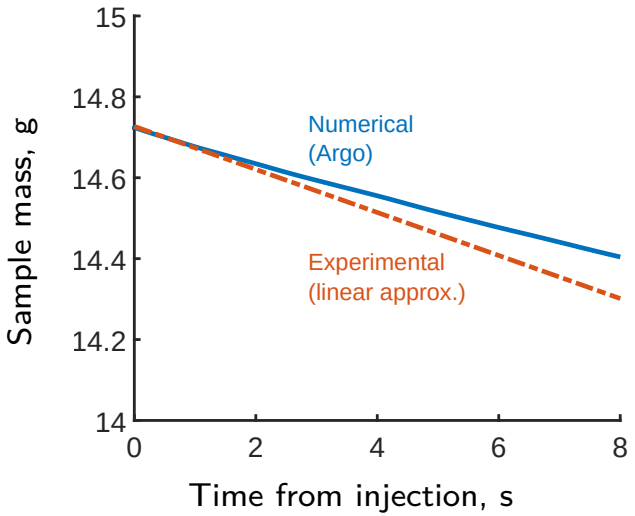

- Analysis of the flow field inside the porous material ($t = 8$ s)

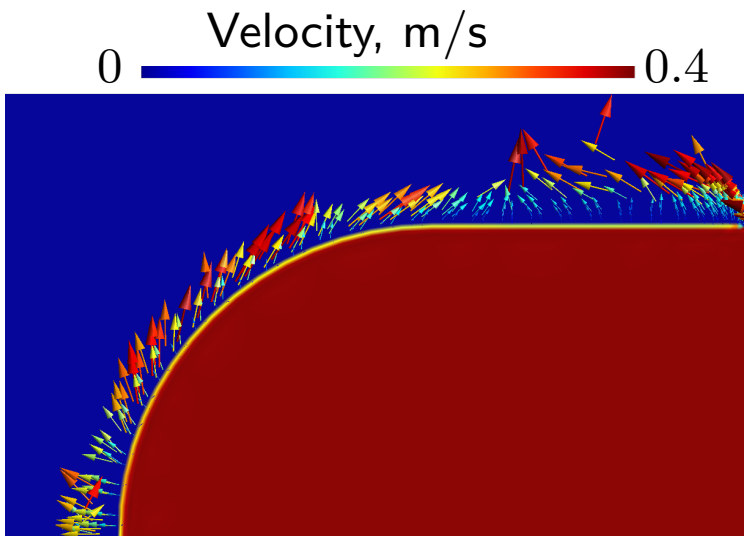

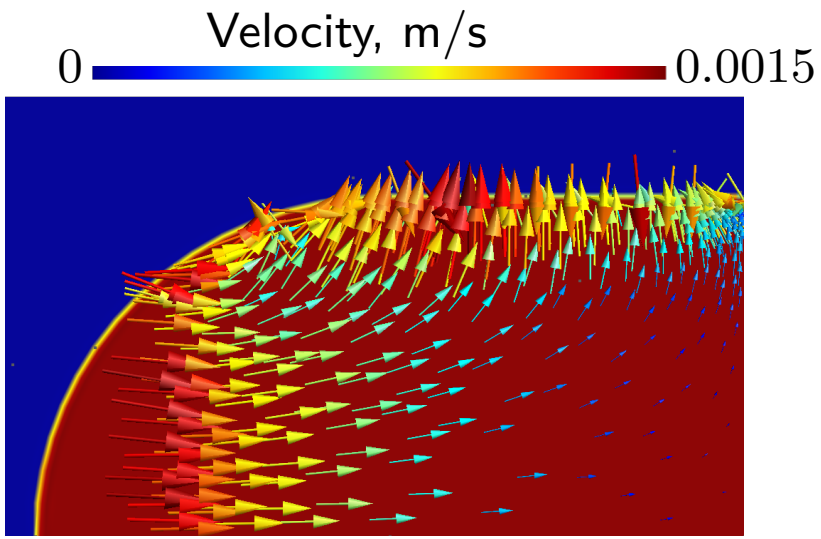

Mass fractions along stagnation line

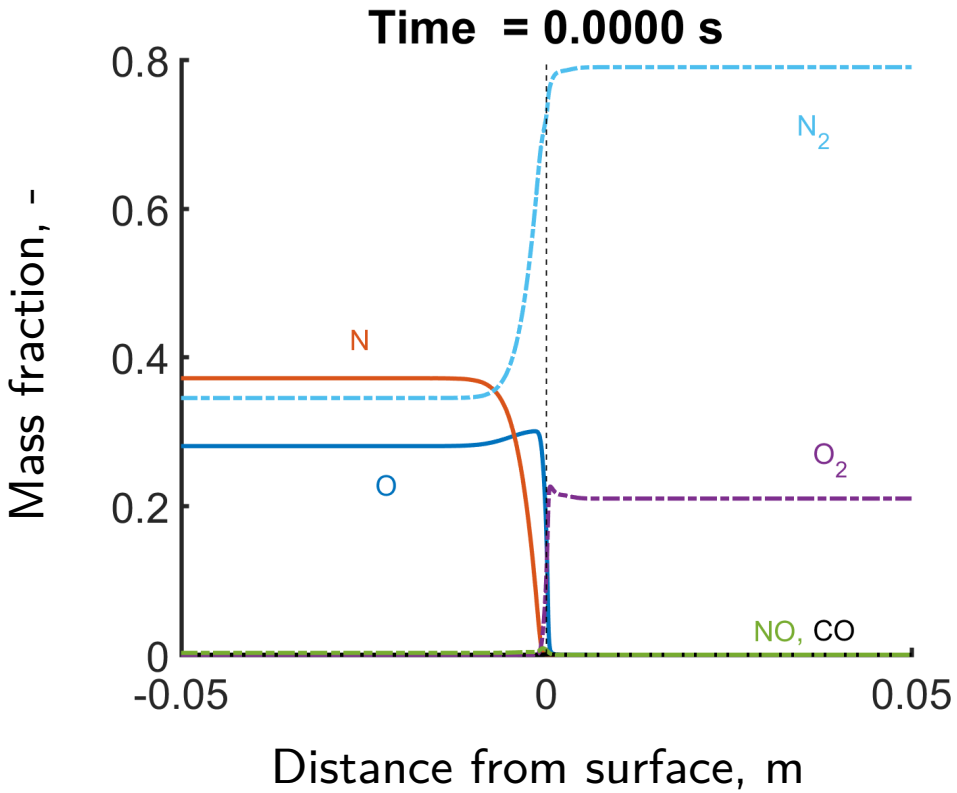

Discussion

- Production of CO mainly at the surface of the material (oxidation with fibers) ➔ surface limited ablation
- Experiments showed also a peak of CN in front of the material and it is therefore suggested to study more products of ablation

Mass fractions along stagnation line

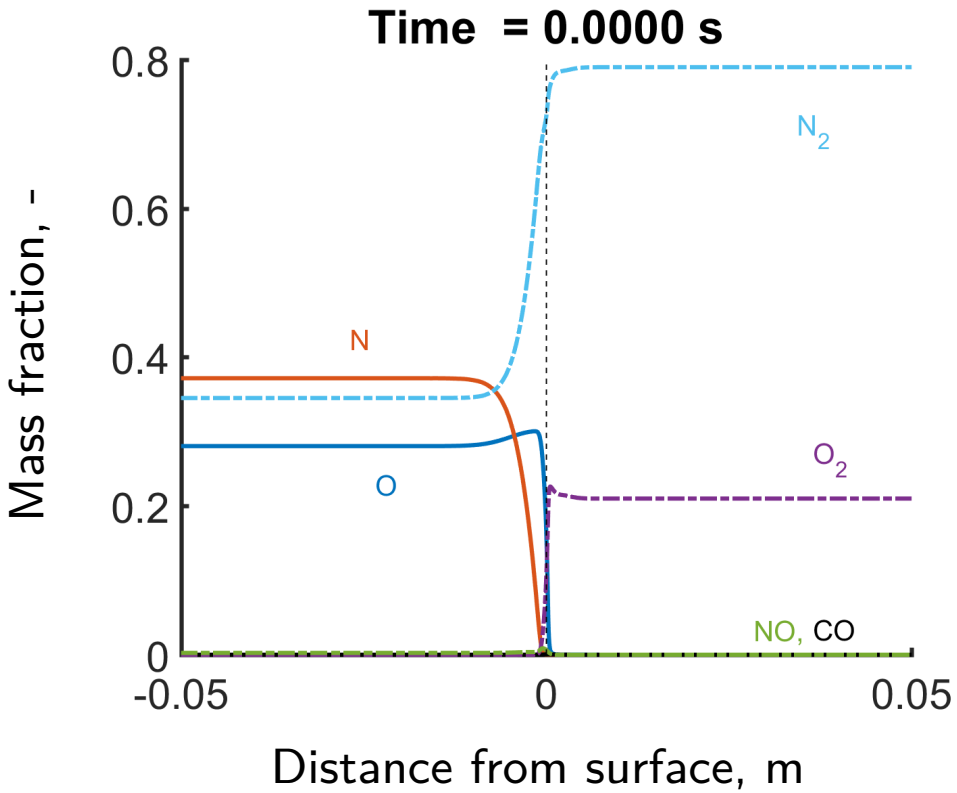

Discussion

- Production of CO mainly at the surface of the material (oxidation with fibers) ➔ surface limited ablation
- Experiments showed also a peak of CN in front of the material and it is therefore suggested to study more products of ablation

Comparison of ablation regime

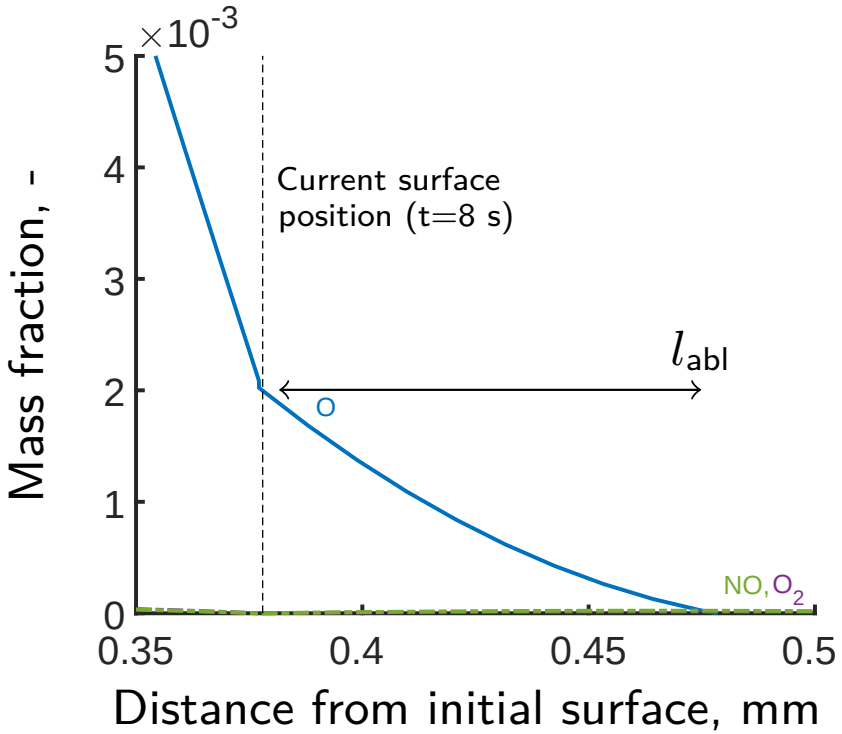

$$Th = \frac{L}{\sqrt{D_{\text{eff}}/(S_f k_f)}} = \frac{L}{l_{\text{abl}}}$$

Surface-limited ablation

$$Th > 50$$

	Experimental	Numerical
Th	360	200

- Surface ablation correctly predicted
- Sensitivity analysis: which definition of the surface position? (50%, 80%, ...of max. density)

Table of Contents

Conclusion and outlook

Previous work:

- Volume-Averaged Navier Stokes solver, fully implicit, discontinuous Galerkin
- Volume ablation experiments were correctly simulated

Conclusion and outlook

Previous work:

- Volume-Averaged Navier Stokes solver, fully implicit, discontinuous Galerkin
- Volume ablation experiments were correctly simulated

In this presentation:

Reproduction of a Plasmatron experiment on a carbon preform test sample by means of the unified approach:

- Surface limited ablation regime reproduced accurately
- Good agreement with experimental data for surface recession
- Good agreement for mass loss (slight underestimate)
- Surface temperature sensitive to the definition of surface position

Conclusion and outlook

Outlook:

- Sensitivity analysis of surface position and uncertainty quantification of other input parameters
- Simulation of different ablation regimes
- Comparison with other classical approaches

Numerical simulation of a non-charring ablator in high-enthalpy flows by means of a unified flow-material solver

P. Schrooyen[1], **J. Coheur**[2,3], A. Turchi[3], K. Hillewaert[1], P. Chatelain[4], T. Magin[3]

[1]Cenaero, Gosselies, Belgium
[2]Université de Liège, Liège, Belgium
[3]von Karman Institute for Fluid Dynamics, Brussels, Belgium
[4]Université Catholique de Louvain-la-Neuve, Louvain-la-Neuve, Belgium

47th AIAA Thermophysics Conference, June 5–9, 2017
Denver, Colorado, USA
TP-02, Ablation I

Bibliography

- G. Duffa. *Ablative Thermal Protection Systems Modeling*. AIAA, Inc., Reston, Virginia, 2013.
- B. Helber. *Material response characterization of low-density ablators in atmospheric entry plasmas*, Ph.D. thesis, Vrije Universiteit Brussel & von Karman Institute, 2016.
- K. Hillewaert, *Development of the discontinuous Galerkin method for large scale/high-resolution CFD and acoustics in industrial geometries*, Ph.D. thesis, Université Catholique de Louvain-la-Neuve, 2013.
- J. Lachaud, I. Cozmuta, N. Mansour. "Multiscale approach to ablation modeling of phenolic impregnated carbon ablators". *Journal of Spacecraft and Rockets*, 47(6):910–921, 2010.
- J. Lachaud, T. Magin, I. Cozmuta and N. Mansour. *A short review of ablative-materials response models and simulation tools*. 7th European Symposium on Aerothermodynamics, Brugge, Belgium, 2011.
- F. Panerai, A. Martin, N. Mansour, S. Sepka, J. Lachaud. "Flow-tube oxidation experiments on the carbon preform of a phenolic-impregnated carbon ablator", *Journal of Thermophysics and Heat Transfer*, 28(2):181–190, 2014.
- P. Schrooyen. *Numercial simulation of aerothermal flows through ablative thermal protection systems*. PhD Thesis. UCL & VKI, 2015.
- P. Schrooyen, K. Hillewaert, T. Magin, P. Chatelain. "Fully implicit discontinuous Galerkin solver to study surface and volume ablation competition in atmospheric entry flows", *International Journal of Heat and Mass Transfer*, 103:108–124, 2016.

Part II

Backup Slides

Mathematical model

Multicomponent diffusion

$$\langle \boldsymbol{J}_i \rangle = -\epsilon_g \langle \rho_i \rangle_g \frac{D_{i,m}}{\eta} \frac{W_i}{W} \nabla X_i + \epsilon_g \langle \rho_i \rangle_g \sum_{k=1}^{N_s} \frac{D_{k,m}}{\eta} \frac{W_k}{W} \nabla X_k$$

- X_i mole fractions, Y_i mass fractions, W molecular weight
- $D_{i,m}$ average diffusion coefficient of one species in the mixture
- η tortuosity: measures the geometric length ratio between the real trajectory of a particle between two points in the porous medium and a straight line. This parameter depends on the architecture of the porous medium and the mean free path

Mathematical model

Drag term

$$F_{\text{drag}} = \frac{1}{dV} \oint_{\partial dV} (-P' \boldsymbol{I} + \boldsymbol{\tau}) \boldsymbol{n} \, dS = \frac{-\mu}{\kappa} \epsilon_g^2 \langle \boldsymbol{u} \rangle_g$$

- μ dynamic viscosity,
- κ permeability: measures the ability of a fluid to flow through the porous material and depends on the microstructure of the material

Mathematical model

Homogeneous chemical reactions

$$\dot{\omega}_i^{\text{hom}} = W_i \sum_{k=1}^{N_r} (\nu''_{ik} - \nu'_{ik}) \left(k_{f,k} \prod_{j=1}^{N_s} \tilde{\rho}_j^{\nu'_{j,k}} - k_{b,k} \prod_{j=1}^{N_s} \tilde{\rho}_j^{\nu''_{j,k}} \right)$$

- W_i molecular weight
- ν_{ik} stoichiometric coefficient
- $k_{f,k}$, $k_{b,k}$ forward and backward reaction rates

Homogeneous reaction rates are computing using the Mutation++ library developed at VKI

J. B. Scoggins and T. E. Magin, "Development of Mutation++: Multicomponent Thermodynamic and Transport Properties for Ionized Plasmas written in C++", *In 11th AIAA/ASME Joint Thermophysics and Heat Transfer Conference*, 2014.

Mathematical model

Heterogeneous chemical reactions

$$\langle \dot{\omega}_i^{\text{het}} \rangle = \frac{1}{dV} \oint_{\partial\Omega_g} \underbrace{k_f^{i,C(s)} \langle \rho_i \rangle_{\text{gs}}}_{\text{constant along fiber surface}} \, dS$$

$$= k_f^{i,C(s)} \langle \rho_i \rangle_{\text{gs}} \underbrace{\frac{1}{dV} \oint_{\partial\Omega_g} dS}_{=A_{\text{w}}/dV \equiv S_f}$$

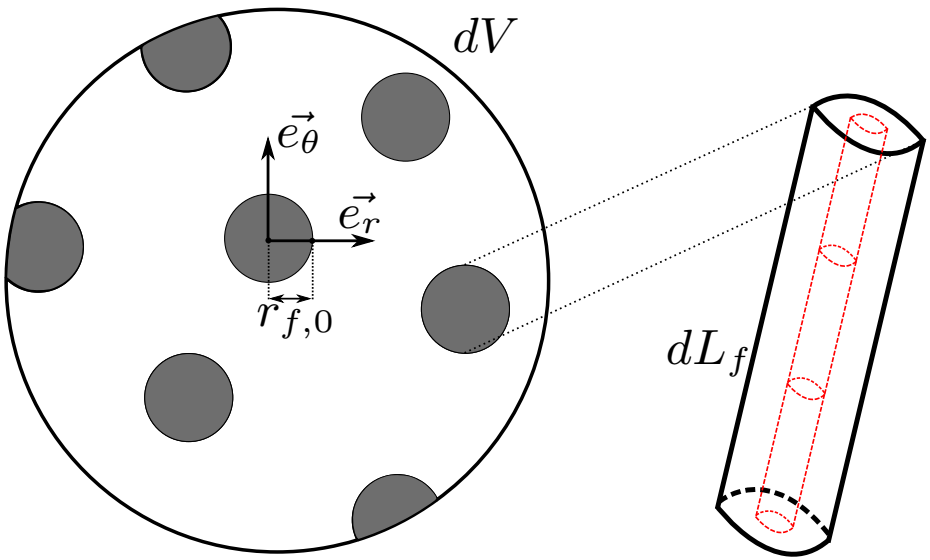

Cylindrical recession

$$S_f = \frac{2}{r_{f,0}} \sqrt{\varepsilon_{s,0} \varepsilon_s}$$

Non-constant fiber reactivity

$$S_f = \gamma \frac{A_w}{dV}$$

(see Schrooyen et al., 2016)

Preliminary analyses

- Residual history

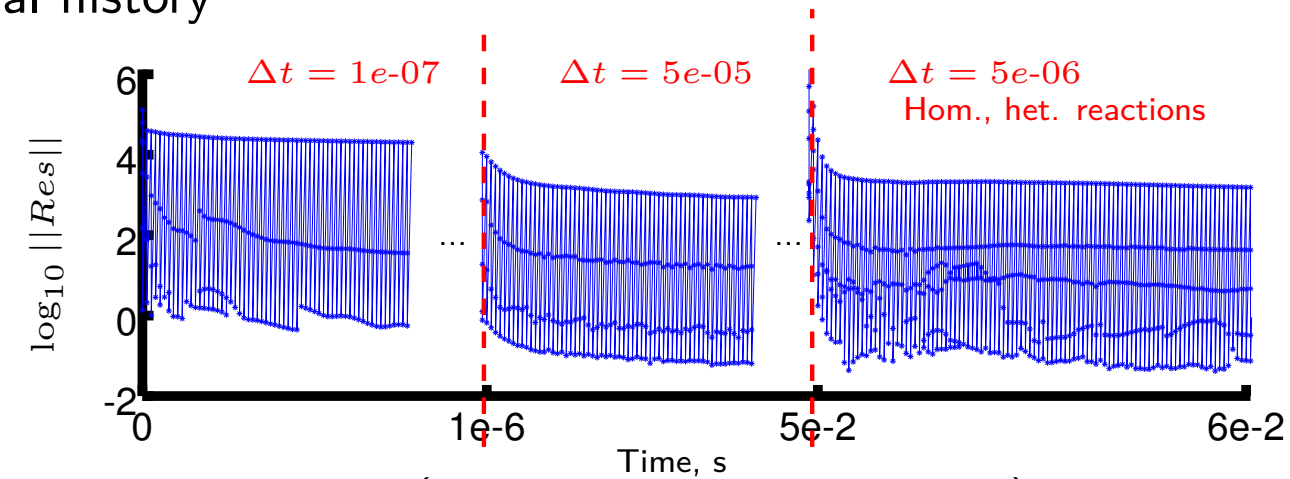

- Analysis of the speedup (VKI cluster *ClusterVision*)

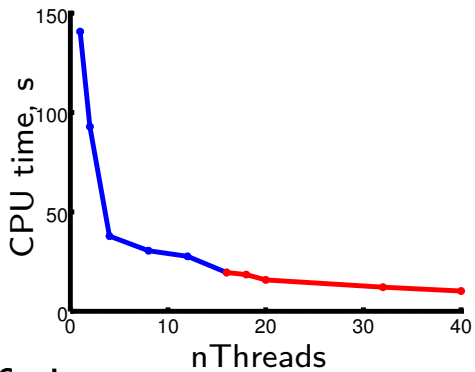

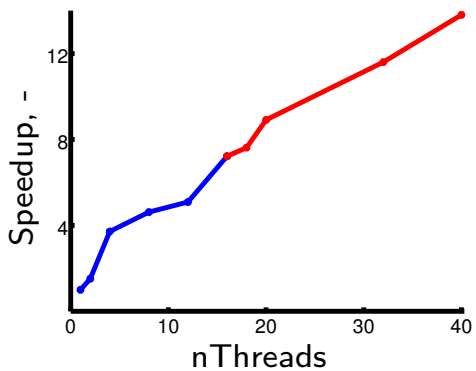

- Summary of the test case

Test Case	Nb of time step	Nb of elemts	Nb of DOF	Nb of CPUs	CPU time
$HS\text{-}A2a$ coarse mesh	198000	1457	$1457 \times 3 \times 10$	12	$\approx$ 3 weeks

Mixture properties and chemical reactions

- 6-components mixture: N, O, NO, N_2, O_2, CO
- Transport and thermo. properties: multicomponent model using Mutation++ as an external library

- Homogeneous reactions

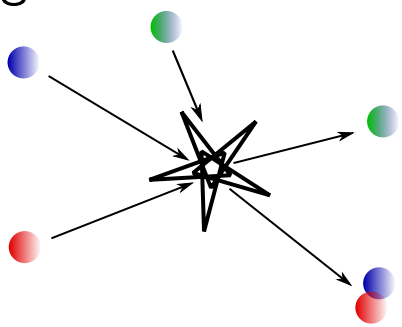

- $N + O + N_2 \rightleftharpoons NO + N_2$
- ...

- Heterogeneous reactions

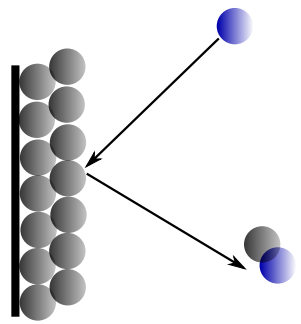

- $2C_{(s)} + O_2 \rightarrow 2\ CO$
- $C_{(s)} + O \rightarrow CO$

HSA2a Results

- Surface temperature

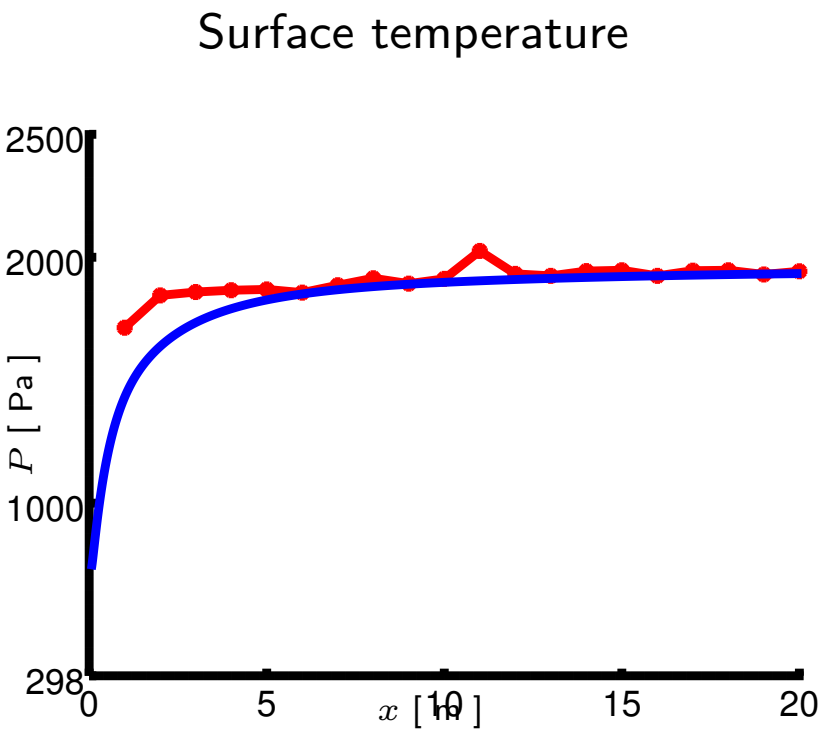

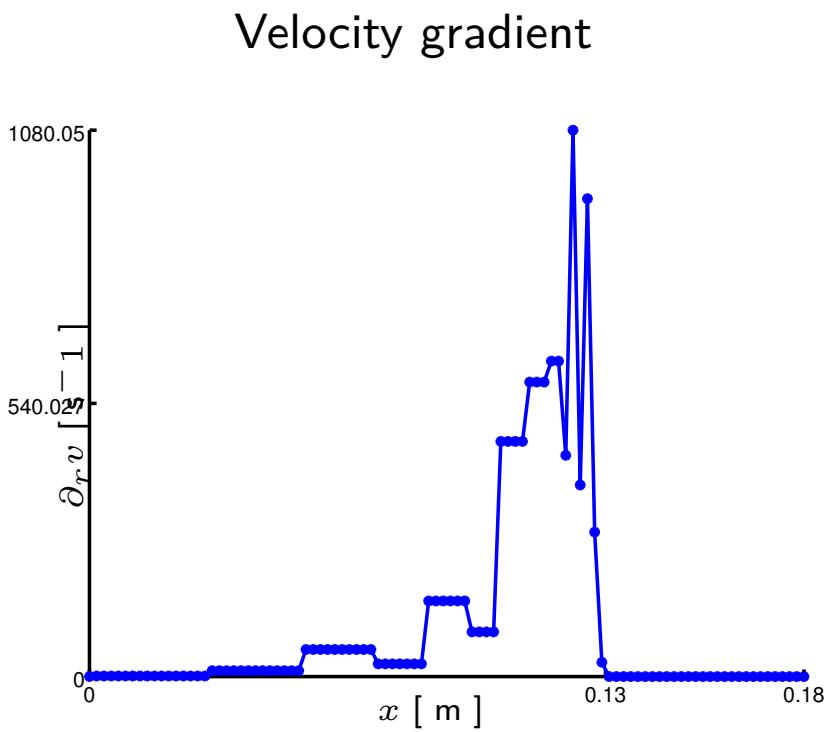

- Experimental results available (Helber, 2016): Stag. surface temperature, mass loss, recession rate, length of ablation

HSA2a Results

- Temperature

Axial velocity along stagn. line

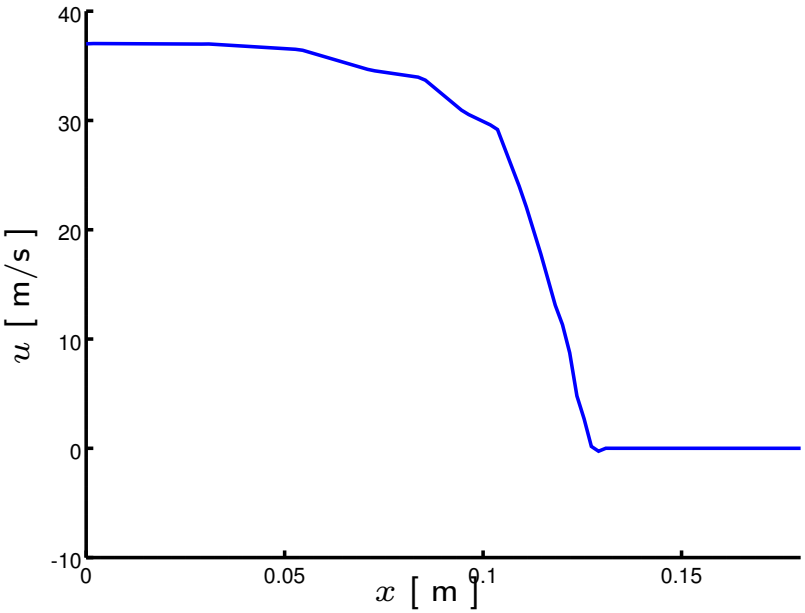

Temperature along stag. line

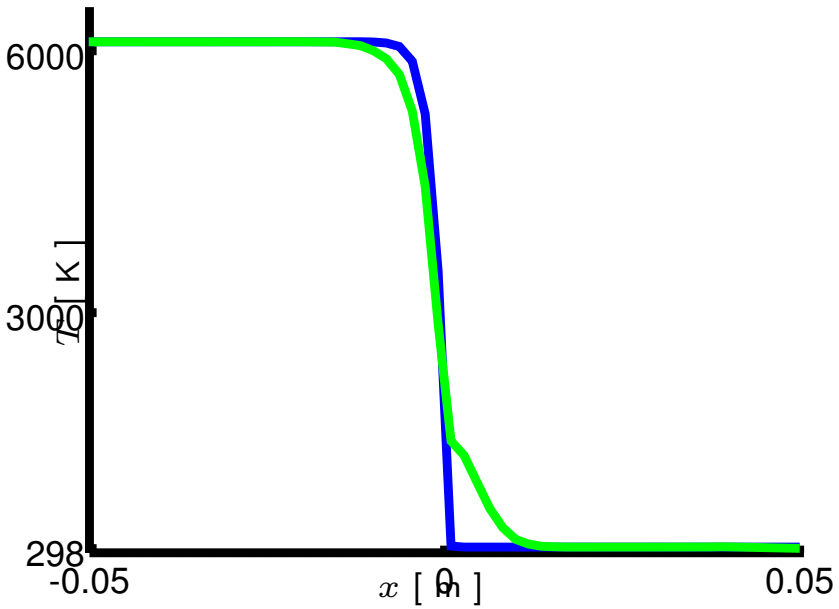

- Experimental results available (Helber, 2016): Stag. surface temperature, mass loss, recession rate, length of ablation

Thermal decomposition of the solid phenolic resin

- During pyrolysis, resin matrix converts into carbon (~ 60 %), releasing gaseous products (~ 40 %)

$$\rho_0 \rightarrow \rho_g + \rho_c$$

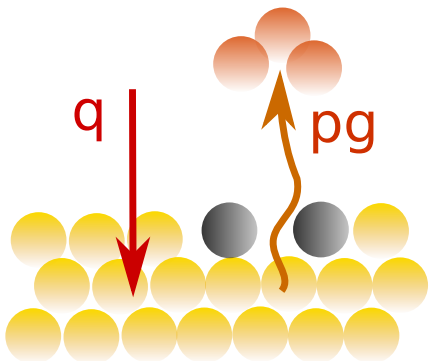

- Goldstein (1969): pyrolysis of the phenolic takes place in two major reactions

$$\frac{d\rho_I}{dt} = -k_I \exp(-E_I/RT) \left(\frac{\rho_I - \rho_c}{\rho_0} \right)^{n_I}, \quad I = A, B$$

- Trick, Saliba, Sandhu (1995, 1997): 4 heterogeneous reactions in the process!

Evolution of matrix volume fraction

- Thermal decomposition of solid species

$$\frac{\partial \langle \rho_m^i \rangle_m}{\partial t} = -A_i \rho_i^v \left(\frac{\rho_i - \rho_i^c}{\rho_i^v} \right)^{n_i} \exp\left(\frac{-E_i}{RT} \right)$$

- Advancement of pyrolysis reaction i

$$\xi_i = \frac{\rho_i^v - \rho_i}{\rho_i^v - \rho_i^c}$$

- Matrix fraction evolves as a linear comb. of resin and charred

$$\varepsilon_m^i \langle \rho_m^i \rangle_m = (1 - \xi_i) \langle \rho_v^i \rangle_m \varepsilon_{mv}^i + \xi_i \langle \rho_c^i \rangle_m \varepsilon_{mv}^i$$

- Mass loss fraction during **p**yrolysis and **c**harred fraction

$$\varepsilon_{mv}^i \langle \rho_v^i \rangle_m = F_p^i \langle \rho_v \rangle_m \varepsilon_{mv}$$
$$\varepsilon_{mv}^i \langle \rho_c^i \rangle_m = F_c^i \langle \rho_v \rangle_m \varepsilon_{mv}$$

Evolution of matrix volume fraction

- Tacot assumption

$$\sum_i \langle \rho_m^i \rangle_m = \langle \rho_m \rangle_m = \langle \rho_{mv} \rangle_m = \langle \rho_{mc} \rangle_m$$

- Summing over all the species

$$\varepsilon_m \langle \rho_m \rangle_m = \varepsilon_{mv} \left(\sum_i^{n_p} F_p^i (1 - \xi_i) + \sum_i^{n_p} \xi_i F_c^i \right)$$

- Porosity

$$\varepsilon = 1 - \varepsilon_f - \varepsilon_m$$

Permeability

- Linear with temperature (from virgin to charred and preform), TACOT properties
- Improvement: TACOT properties for virgin and charred, Carman-Kozeny for preform

Tortuosity

Thermal conductivity

- TACOT properties

Gaseous species production

Emissivity of the surface

Material properties for unified flow approach

- No thermodynamics properties for the pure solid phase are available in open literature

➔ Adaptation of the usual TACOT properties using `Mutation++` with air

: Modified virgin properties
: Modified charred properties
: Vrigin TACOT properties
: Charred TACOT properties